Rapid Communications

Bound states in the continuum of higher-order topological insulators

Wladimir A. Benalcazar and Alexander Cerjan
Department of Physics, The Pennsylvania State University, University Park, Pennsylvania 16802, USA

(Received 27 August 2019; revised manuscript received 12 February 2020; accepted 3 April 2020; published 28 April 2020)

We show that lattices with higher-order topology can support corner-localized bound states in the continuum (BICs). We propose a method for the direct identification of BICs in condensed matter settings and use it to demonstrate the existence of BICs in a concrete lattice model. Although the onset for these states is given by corner-induced filling anomalies in certain topological crystalline phases, additional symmetries are required to protect the BICs from hybridizing with their degenerate bulk states. We demonstrate the protection mechanism for BICs in this model and show how breaking this mechanism transforms the BICs into higher-order topological resonances. Our work shows that topological states arising from the bulk-boundary correspondence in topological phases are more robust than previously expected, expanding the search space for crystalline topological phases to include those with boundary-localized BICs or resonances.

DOI: 10.1103/PhysRevB.101.161116

Topological insulators exhibit robust quantized electromagnetic phenomena with exotic boundary manifestations. A paradigmatic example is the family of topological insulators with quantized dipole moments in their bulk and charge fractionalization at their boundaries [1–4]. This property of boundary charge fractionalization has recently been extended through the discovery of quantized electric multipole insulators [5,6] and, more generally, nth-order topological insulators in n dimensions, all of which host corner fractional charges in two and three dimensions (2D and 3D) [5–14].

Among higher-order topological insulators (HOTIs) with fractional corner charges, those with additional chiral or particle-hole symmetries also host robust corner-bound states at midgap [5,7,15]. This property makes them attractive because these topological states are easy to access experimentally due to their spectral isolation and are maximally confined [16–18]. Recently, it has also been shown that these states present nontrivial braiding properties [19,20].

Requiring a bulk bandgap to find spectrally isolated topological states rules out potential materials and metamaterials which otherwise possess all of the necessary crystalline symmetries to exhibit a higher-order topological phase. Yet, in principle, spectral isolation is not necessary for the existence of localized bound states. Bound states that coexist with degenerate extended ones, commonly known as bound states in the continuum (BICs), have been found across a variety of other physical systems, including quantum systems [21–24], water waves [25–30], acoustics [31–36], and photonics [37–55].

Thus, the natural question to consider is, do topological crystalline insulators with fractional corner charges still possess corner-localized states in the absence of a gap? And, if so, what protects these states from hybridizing with bulk states at the same energy? If such protected corner-localized modes do exist, they are condensed matter realizations of BICs, as they would localize to a zero-dimensional region of the system despite the existence of the background of continuum states in the bulk of the material.

Previous studies on BICs consider systems which are coupled to scattering channels in the surrounding continuum that satisfy radiative boundary conditions, rendering their Hamiltonians non-Hermitian by allowing energy to radiate away. In contrast, condensed matter systems, being closed systems, have presented challenges in even defining the appropriate criteria for diagnosing the existence of BICs, which only a few previous studies have attempted to address [18,56,57].

In this Rapid Communication, we challenge the notion that boundary states of a topological phase will inevitably mix with bulk bands that are degenerate in energy with them. Instead, we show that boundary states can remain localized despite being degenerate with bulk bands and, as such, constitute condensed-matter realizations of BICs. To do so, we draw inspiration from open systems to devise a method that allows the identification of BICs in closed crystalline systems. By adding fictitious non-Hermitian terms to the Hamiltonian of the crystal, and in the correct limits, this method identifies BICs in the *original* system as the isolated states with only purely real energies in the complex energy spectrum. Equipped with this tool, we study a concrete model of a 2D HOTI without a bulk gap at zero energy and conclusively demonstrate the existence of zero-energy corner-localized BICs. We further show that the protection of BICs in this lattice exists beyond separability [58,59] and depends only on the preservation of crystalline and chiral symmetries. In the absence of these symmetries (but still preserving those which protect the HOTI phase), the BICs mix with their degenerate bulk states to become higher-order topological resonances, i.e., sets of states mostly localized at corners that nevertheless also have a delocalized bulk component, and which constitute the most general spectroscopic expression of a corner-filling anomaly and corner fractional charge.

Lattice and its topological phases. The lattice we consider is shown in Fig. 1(a) and consists of four sites per unit cell with dimerized nearest-neighbor couplings of amplitude 1 (solid lines) and t (dashed lines) [60]. For the basis indicated

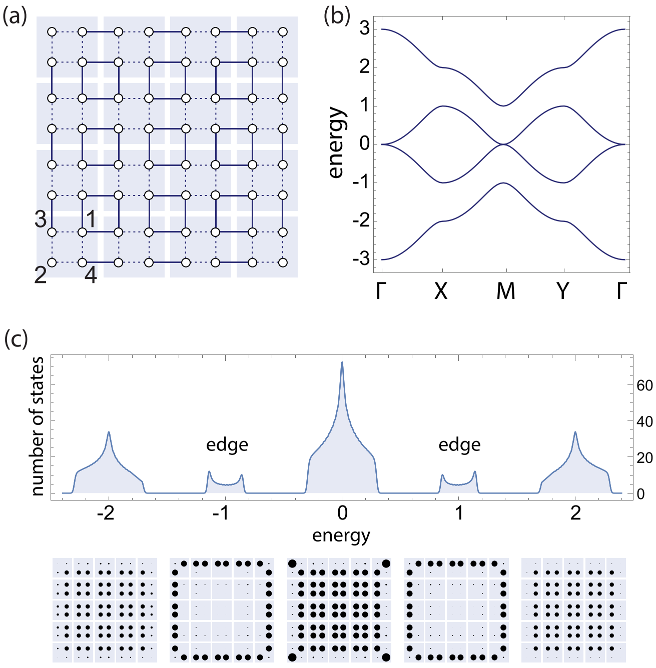

FIG. 1. Characterization of the model lattice with closed and open boundaries. (a) Lattice with Bloch Hamiltonian in Eq. (1). (b) Bulk energy bands along high-symmetry lines of the Brillouin zone for a lattice with periodic boundaries, for $t = 0.5$. (c) Density of states when boundaries are open in both directions ($n = 20$, $t = 0.15$). The lower panels indicate the probability densities per band ($n = 5, t = 0.15$).

by the numbers in Fig. 1(a), the Bloch Hamiltonian of the system is

$$h(\mathbf{k}) = \begin{pmatrix} 0 & Q \\ Q^\dagger & 0 \end{pmatrix}, \quad Q = \begin{pmatrix} t + e^{ik_x} & t + e^{ik_y} \\ t + e^{-ik_y} & t + e^{-ik_x} \end{pmatrix}. \qquad (1)$$

Its bulk energy bands are shown in Fig. 1(b). This Hamiltonian has chiral symmetry, $\{\Pi, h(\mathbf{k})\} = 0$, where $\Pi = \sigma_z \otimes \mathbb{I}_{2\times 2}$ is the chiral operator, as well as C_{4v} symmetry. As such, the spectrum is symmetric around zero energy due to chiral symmetry (see Ref. [61]) and the two middle bands are twofold degenerate at the $\mathbf{\Gamma}$ and $\mathbf{M}$ points of the Brillouin zone as they adopt the two-dimensional irreducible representation of C_{4v}. Thus, due to the simultaneous presence of chiral and C_{4v} symmetries, the lattice will always have gapless bulk energy bands at zero energy.

The presence of C_{4v} symmetry in the lattice distinguishes two topological phases. For $|t| < 1$, all the bands in the lattice are in a topological phase, with different C_{4v} (C_{2v}) representations at $\mathbf{M}$ ($\mathbf{X}$ and $\mathbf{X}'$) relative to $\mathbf{\Gamma}$. On the other hand, for $|t| > 1$, all the bands are in a trivial phase, with equal symmetry representations at all high-symmetry points (HSPs) of the Brillouin zone. The symmetry representations at all HSPs for both phases and their associated symmetry indicator topological invariants are shown in Ref. [61]. At $|t| = 1$, the phase transition occurs by closing both bulk gaps at $\mathbf{X}$, $\mathbf{X}'$, and $\mathbf{M}$, exchanging the representations at these three HSPs.

This model has been recently studied in the context of charge fractionalization in higher-order topological crystalline insulators [11]. In the topological phase, the Wannier centers in all the bands localize at the maximal Wyckoff position $1b$ (corner of the unit cell), while in the trivial phase the Wannier centers in all the bands are localized at the maximal Wyckoff position $1a$ (center of the unit cell). The displacement of the Wannier centers relative to the center of their unit cells generates dipole moments per unit length quantized by C_2 symmetry to $\mathbf{P} = (\frac{e}{2}, \frac{e}{2})$ in the first and fourth bands of the lattice [11]. These quantized dipole moments are accompanied by two edge energy bands (i.e., bands with edge-localized states) spectrally isolated from the bulk energy bands [Fig. 1(c)].

In addition to the dipole moments, the topological phase has a corner-induced filling anomaly [11,62] with secondary topological indices protected by C_4 symmetry $Q^{(4)} = \frac{1}{4}, \frac{1}{2}, \frac{1}{4}$ for the first, middle, and upper band, respectively [11] (see Ref. [61] for details), which capture the second-order topological character of the bands. When boundaries are open in both directions, the filling anomaly accounts for a reorganization in the number of states across bands relative to when boundaries are periodic [11]. This reorganization is evident in the lack of homogeneity in the probability density functions shown in the lower panels of Fig. 1(c). In particular, the central band shows pronounced support over the corner unit cells and, as we will see, are associated with the existence of corner BICs.

Bound states in the continuum. In electronic systems, a nonzero filling anomaly indicates the fractionalization of the corner charge, which is the robust physical manifestation of higher-order nontrivial topology. A filling anomaly, however, does not necessarily imply the existence of zero-energy corner states. In the presence of bulk states degenerate at zero energy, as in this model, we would expect the corner and bulk states to hybridize and form corner-localized resonances, whose localization does not exponentially attenuate into the bulk completely as they would have nonzero bulk support. However, if states exponentially confined to corners exist as stand-alone eigenstates of the system despite the existence of degenerate bulk states, we will have corner-localized BICs.

We can directly test for the existence of corner BICs by dividing the lattice into two regions: a small region that we leave intact which we call the "system" $\mathcal{S}$, comprising the four square regions located at the corners of the lattice, each of size $n_s \times n_s$ unit cells, and a large region called the "environment" $\mathcal{R}$, containing all of the unit cells not in $\mathcal{S}$ (inset of Fig. 2). To the environment, we add the non-Hermitian on-site terms

$$h_{\text{loss}} = -i\kappa \sum_{\mathbf{r}\in\mathcal{R}} \sum_{\alpha=1}^{4} c^\dagger_{\mathbf{r},\alpha} c_{\mathbf{r},\alpha}, \quad 0 < \kappa \ll 1, \qquad (2)$$

which amount to uniform losses in all the sites in the environment. If we now inject an initial wave function $\psi(0)$ into the lattice, it will evolve as $\psi(t) = e^{-iHt}\psi(0)$ (from now on we set $\hbar = 1$), where H is the Hamiltonian containing both the Hermitian Hamiltonian, Eq. (1), and the non-Hermitian terms, Eq. (2).

Due to the losses in the environment and the fact that all sites in the lattice are coupled, we expect $|\psi(t)|^2$ to decrease over time. However, if corner-localized bound states exist in the continuum of the lattice, and for system sizes larger than the exponential confinement of the bound states, the losses of a wave function injected at the bound state will be heavily

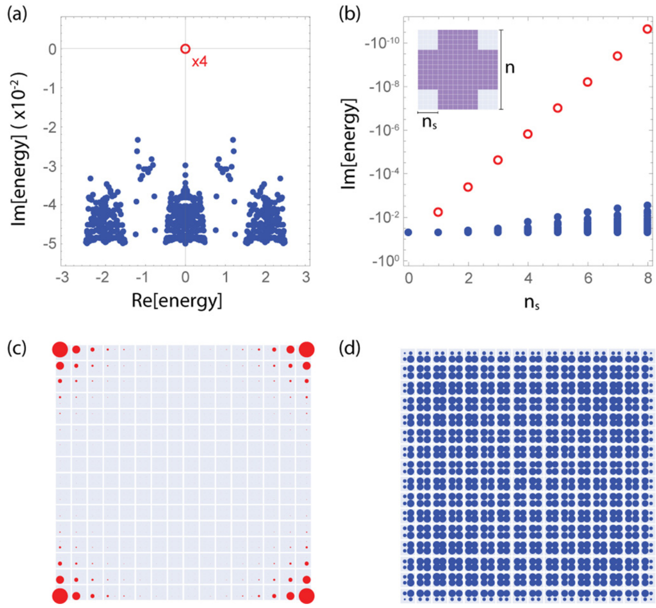

FIG. 2. Probing the existence of bound states in the continuum by adding the non-Hermitian term, Eq. (2), to the lattice in Fig. 1(a) in the topological phase. (a) Complex energies. (b) Imaginary component of the energies as a function of system size (the inset shows the shapes of the "system" and "environment" regions in gray and purple, respectively). In (a) and (b), the red open circle is the fourfold degenerate energy of the bound states in the continuum with support at the corners, and the blue solid circles have eigenstates with support in bulk or edges. (c), (d) Probability density function of (c) the BICs and (d) the bulk states *at zero real energy*. In (c) and (d), the area of the circles is proportional to the amplitude $|\psi|$ of the states. In (a), (c), and (d), $n = 16$ unit cells, $n_s = 3$ unit cells. In (b), $n = 32$. In all plots, $\kappa = -5 \times 10^{-2}$ and $t = 0.25$.

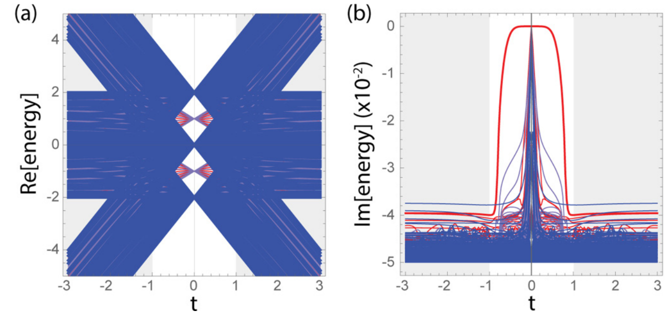

FIG. 3. Complex energies in the lattice as a function of the hopping amplitude t. Shaded and nonshaded regions correspond to the trivial and topological phases, respectively. (a) Real component of the energies. (b) Imaginary component of the energies. Both plots show the overlapped spectra of three configurations: periodic boundaries in both directions (blue), periodic boundary only along one direction (purple), and open boundaries in both directions (red). Blue spectra are on top of purple spectra, both of which are on top of red spectra. For all plots, $n = 16$, $n_s = 3$, $\kappa = -5 \times 10^{-2}$.

suppressed. This loss suppression manifests in the propagator e^{-iHt} by the existence of eigenstates of the Hamiltonian with close-to-real energies and bound to the corners (more precisely, the imaginary component of the complex energy of the bound states should exponentially approach zero with increasing system size).

This exact behavior of the energies of the system is observed in Fig. 2, which shows corner-localized bound states in the topological phase of our model. Figure 2(a) shows the complex energies of the Hamiltonian H, in which four energies are close to being purely real (red open circles), while all of the other energies have a nonvanishing imaginary component (solid blue circles). These four nearly real eigenvalues are shown in Fig. 2(b) to approach zero imaginary components exponentially fast with increasing system size. As expected, the real energies have eigenstates bound to the corners [Fig. 2(c)]. Crucially, these corner bound states are embedded in the continuum of energies of the central bulk energy band, as can be seen in the cumulative probability density function of all eigenstates with zero real energy other than the four corner bound states [Fig. 2(d)], which confirms that the zero-energy corner states are BICs.

BICs as a signature of the topological phase. The penetration of the BICs into the bulk is exponentially suppressed as expected for topological states obeying a bulk-boundary correspondence [63]. Indeed, the corner BICs are a topological signature exclusive of the topological phase and its associated filling anomaly. When the filling anomaly vanishes, so do the BICs.

This is seen in Fig. 3, which shows the real and imaginary energies as a function of the hopping amplitude t. In the real spectrum [Fig. 3(a)] it is possible to see the appearance of in-gap edge-localized states in the topological phase when boundaries are open in one direction (purple bands) [64] (In Fig. 3(a), the phase transitions at $|t| = 1$ are not visible due to indirect gap closings in the bulk, which start to occur at $t = 0.5$ [c.f. Fig. 1(b)]). Here, we focus on corner-bound states because they do not have any spectral isolation at any point in the real energy spectrum and their existence is far from evident. Indeed, we saw that the bound states are embedded in the continuum of the central energy band, and can be separated only in *complex energy* when losses are added to the environment $\mathcal{R}$. Under this prescription, only the imaginary component of the spectrum allows the identification of the corner-bound states. These are shown as the red line at zero imaginary energy in the topological phase ($|t| < 1$) in Fig. 3(b). Notice the sharp transition of the BICs into lossy states as the system approaches the phase transition point ($|t| = 1$). In the trivial phase ($|t| > 1$), the BICs disappear as the filling anomaly vanishes.

Symmetry protection of the BICs. Any spatial symmetry that fixes the Wannier center of the topological phase to the maximal Wyckoff position $1b$, such as C_2 or C_4 symmetries, protects the corner filling anomaly. However, additional symmetries are required to protect the BICs from mixing with other degenerate bulk states to form resonances. In our model, both C_{4v} and chiral symmetries are required to protect the BICs, as we will show now.

In the bulk, all states at zero energy take the two-dimensional representation E of C_{4v} (see Table S2 in Ref. [61] for a definition of the representations). Degenerate to these are the four corner states which, as a whole, form the representation $A_1 \oplus B_2 \oplus E$. The A_1 and B_2 corner states cannot mix

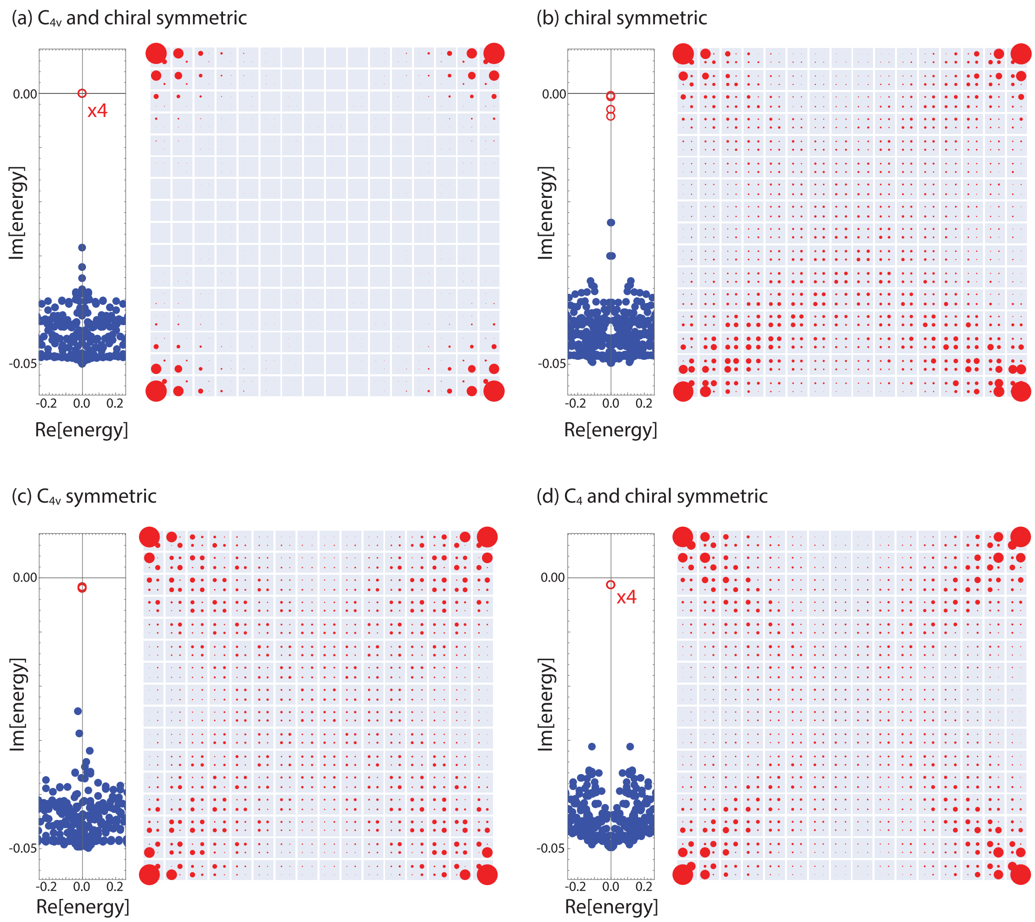

FIG. 4. Breaking the symmetries that protect the BICs. Energy eigenvalues (left panels) and probability densities of the four states whose energies have their imaginary components closest to zero (right panels) under perturbations that preserve certain symmetries: (a) C_{4v} and chiral symmetries, (b) only chiral symmetry, (c) only C_{4v} symmetry, and (d) C_4 and chiral symmetries. In the energy plots, the red open circles correspond to the four energies with imaginary components closest to zero (possibly degenerate). Only (a) has BICs; (b), (c), and (d) have corner-localized topological resonances. For all plots, $n = 16$, $n_s = 3$, $\kappa = -5 \times 10^{-2}$, and $t = 0.25$.

with the E bulk states as they have incompatible symmetry representations. However, the E corner and E bulk states can in principle mix. Consider the combinations of corner states $|C_+\rangle = \frac{1}{2}(1, -1, i, -i)^T$ and $|C_-\rangle = \frac{1}{2}(1, -1, -i, i)^T$ that form a basis for the E irreducible representation of corner states, where the entries correspond to the corner states localized at the top right, bottom left, top left, and bottom right corners, respectively. Since $|C_\pm\rangle$ form a basis for a 2D irrep, they are degenerate in energy as long as C_{4v} is preserved. This basis is convenient because, in the presence of chiral symmetry, $|C_\pm\rangle$ are chiral partners of each other, i.e., $|C_+\rangle = \Pi|C_-\rangle$ and vice versa, from which it follows that these two states should have energies of opposite sign, $\epsilon, -\epsilon$ (see Ref. [61]). Thus, under C_{4v} and chiral symmetry, $|C_\pm\rangle$ must both have $\epsilon = 0$. By the same argument, all bulk states that fall into the E representation of C_{4v} must have $\epsilon = 0$ under chiral symmetry.

Now, consider a possible hybridization of the corner states $|C_\pm\rangle$ and the bulk states $|B_\pm\rangle$ (that form the E representations of C_{4v}) into $|\psi_1\rangle = \alpha(|B_+\rangle + \beta|C_\pm\rangle)$, where $\alpha = 1/\sqrt{1+|\beta|^2}$. Due to C_{4v}, there is another state $|\psi_2\rangle = \alpha(|B_-\rangle + \beta|C_\mp\rangle)$ degenerate to $|\psi_1\rangle$. The crucial observation is that $|\psi_1\rangle$ and $|\psi_2\rangle$ are chiral partners of each other, and as such these hybridized states have zero energy. Thus, the states $|\psi_{1,2}\rangle$ are merely arbitrary choices in the highly degenerate subspace of zero energy and do not represent a physical unbreakable hybridization into resonant eigenstates. The prescription for the detection of BICs that we propose here is then sufficient to isolate the corner BICs from the rest of degenerate bulk states.

In the absence of either chiral or C_{4v} symmetry, the hybridized states $|\psi_{1,2}\rangle$ are not pinned to zero energy and are thus free to become eigenstates of the system not susceptible to being separated into their corner and bulk constituents (Fig. 4). The inseparable hybridized states, having support in both the corner and the bulk, will eventually attenuate in the presence of loss in the environment $\mathcal{R}$, which manifests by a nonzero imaginary component of their energies. Some of these states are in principle long-lived as they may have more support in the corners rather than in the bulk, and thus constitute resonances of the system. In Fig. 4 we show the conversion of BICs into resonances as we add perturbations to the original Hamiltonian in Eq. (1) that break the simultaneous C_{4v} and chiral symmetries down to only specific indicated symmetries. The perturbations consist of random hopping terms up to next-nearest-neighbor unit cells that nevertheless preserve the desired symmetries, as detailed in Ref. [61].

In previous studies, one of the possible mechanisms for creating BICs has been attributed to the *separability* of the Hamiltonian into k_x and k_y dependent parts, i.e., $h(k_x, k_y) = h_x(k_x) + h_y(k_y)$ [58,59]. Here, we show that BICs are protected beyond separability. Specifically, Fig. 4(a) has added perturbations that put the overall Hamiltonian in a nonseparable form while still hosting BICs due to the preservation of C_{4v} and chiral symmetries. We also notice that in all cases in Fig. 4 the filling anomaly is preserved and in Figs. 4(a), 4(c) and 4(d), the Wannier centers are still fixed by symmetry to the maximal Wyckoff position 1b. Thus, here we verify that additional symmetries to those required to protect the topological phase and its filling anomaly are required to protect BICs. Topological resonances, however, will generally exist for the symmetries that protect the topological phase, with a quality factor inversely proportional to the amplitude of the imaginary component of their energies. The recent work of Ref. [57] introduces unrestricted (i.e., symmetry-breaking) noise to their system. Thus, we expect that their numerical method for finding corner-localized states is incapable of properly distinguishing BICs from resonances.

Our demonstration that corner-localized modes exist in HOTIs even in the absence of a bulk bandgap expands the search space (design space) for topological materials (topological metamaterials). Moreover, the unique property of coexistence between BICs and bulk states offers an alternative playground for possible applications of topological phenomena.

Acknowledgments. We are grateful for interesting discussions with Mikael Rechtsman, Jonathan Guglielmon, S. N. Kempkes, and Cristiane Morais Smith. W.A.B. is thankful for the support of the Eberly Postdoctoral Fellowship at the Pennsylvania State University. A.C. acknowledges the support of the National Science Foundation under Grants No. ECCS-1509546 and No. DMS-1620422 as well as the Charles E. Kaufman Foundation under Grant No. KA2017-91788.

[1] W. P. Su, J. R. Schrieffer, and A. J. Heeger, Solitons in Polyacetylene, Phys. Rev. Lett. **42**, 1698 (1979).

[2] G. van Miert, C. Ortix, and C. M. Smith, Topological origin of edge states in two-dimensional inversion-symmetric insulators and semimetals, 2D Mater. **4**, 015023 (2016).

[3] J.-W. Rhim, J. Behrends, and J. H. Bardarson, Bulk-boundary correspondence from the intercellular Zak phase, Phys. Rev. B **95**, 035421 (2017).

[4] G. van Miert and C. Ortix, Excess charges as a probe of one-dimensional topological crystalline insulating phases, Phys. Rev. B **96**, 235130 (2017).

[5] W. A. Benalcazar, B. A. Bernevig, and T. L. Hughes, Quantized electric multipole insulators, Science **357**, 61 (2017).

[6] W. A. Benalcazar, B. A. Bernevig, and T. L. Hughes, Electric multipole moments, topological multipole moment pumping, and chiral hinge states in crystalline insulators, Phys. Rev. B **96**, 245115 (2017).

[7] Z. Song, Z. Fang, and C. Fang, $(d-2)$-Dimensional Edge States of Rotation Symmetry Protected Topological States, Phys. Rev. Lett. **119**, 246402 (2017).

[8] B. J. Wieder and B. A. Bernevig, The axion insulator as a pump of fragile topology, arXiv:1810.02373.

[9] G. van Miert and C. Ortix, Higher-order topological insulators protected by inversion and rotoinversion symmetries, Phys. Rev. B **98**, 081110(R) (2018).

[10] M. Ezawa, Minimal models for Wannier-type higher-order topological insulators and phosphorene, Phys. Rev. B **98**, 045125 (2018).

[11] W. A. Benalcazar, T. Li, and T. L. Hughes, Quantization of fractional corner charge in C_n-symmetric higher-order topological crystalline insulators, Phys. Rev. B **99**, 245151 (2019).

[12] E. Lee, R. Kim, J. Ahn, and B.-J. Yang, Two-dimensional higher-order topology in monolayer graphdiyne, npj Quantum Mater. **5**, 1 (2020).

[13] X.-L. Sheng, C. Chen, H. Liu, Z. Chen, Z.-M. Yu, Y. X. Zhao, and S. A. Yang, Two-Dimensional Second-Order Topological Insulator in Graphdiyne, Phys. Rev. Lett. **123**, 256402 (2019).

[14] F. Schindler, M. Brzezińska, W. A. Benalcazar, M. Iraola, A. Bouhon, S. S. Tsirkin, M. G. Vergniory, and T. Neupert, Fractional corner charges in spin-orbit coupled crystals, Phys. Rev. Research **1**, 033074 (2019).

[15] W. A. Benalcazar, Jeffrey C. Y. Teo, and T. L. Hughes, Classification of two-dimensional topological crystalline superconductors and Majorana bound states at disclinations, Phys. Rev. B **89**, 224503 (2014).

[16] J. Noh, W. A. Benalcazar, S. Huang, M. J. Collins, K. P. Chen, T. L. Hughes, and M. C. Rechtsman, Topological protection of photonic mid-gap defect modes, Nat. Photonics **12**, 408 (2018).

[17] C. W. Peterson, W. A. Benalcazar, T. L. Hughes, and G. Bahl, A quantized microwave quadrupole insulator with topologically protected corner states, Nature (London) **555**, 346 (2018).

[18] X. Ni, M. Weiner, A. Alù, and A. B. Khanikaev, Observation of higher-order topological acoustic states protected by generalized chiral symmetry, Nat. Mater. **18**, 113 (2019).

[19] J. Noh, T. Schuster, T. Iadecola, S. Huang, M. Wang, K. P. Chen, C. Chamon, and M. C. Rechtsman, Braiding photonic topological zero modes, arXiv:1907.03208.

[20] T. E. Pahomi, M. Sigrist, and A. A. Soluyanov, Braiding Majorana corner modes in a two-layer second-order topological insulator, arXiv:1904.07822.

[21] J. von Neumann and E. Wigner, Über merkwürdige diskrete eigenwerte, Phys. Z. **30**, 465 (1929).

[22] R. L. Schult, D. G. Ravenhall, and H. W. Wyld, Quantum bound states in a classically unbound system of crossed wires, Phys. Rev. B **39**, 5476 (1989).

[23] N. Moiseyev, Suppression of Feshbach Resonance Widths in Two-Dimensional Waveguides and Quantum Dots: A Lower Bound for the Number of Bound States in the Continuum, Phys. Rev. Lett. **102**, 167404 (2009).

[24] L. S. Cederbaum, R. S. Friedman, V. M. Ryaboy, and N. Moiseyev, Conical Intersections and Bound Molecular States Embedded in the Continuum, Phys. Rev. Lett. **90**, 013001 (2003).

[25] F. Ursell, Trapping modes in the theory of surface waves, Math. Proc. Cambridge Philos. Soc. **47**, 347 (1951).
[26] D. S. Jones, The eigenvalues of $\nabla^2 u + \lambda u = 0$ when the boundary conditions are given on semi-infinite domains, Math. Proc. Cambridge Philos. Soc. **49**, 668 (1953).
[27] M. Callan, C. M. Linton, and D. V. Evans, Trapped modes in two-dimensional waveguides, J. Fluid Mech. **229**, 51 (1991).
[28] C. H. Retzler, Trapped modes: An experimental investigation, Appl. Ocean Res. **4**, 249 (2001).
[29] P. J. Cobelli, V. Pagneux, A. Maurel, and P. Petitjeans, Experimental observation of trapped modes in a water wave channel, Europhys. Lett. **88**, 20006 (2009).
[30] P. J. Cobelli, V. Pagneux, A. Maurel, and P. Petitjeans, Experimental study on water-wave trapped modes, J. Fluid Mech. **666**, 445 (2011).
[31] R. Parker, Resonance effects in wake shedding from parallel plates: Some experimental observations. J. Sound Vib. **4**, 62 (1966).
[32] R. Parker, Resonance effects in wake shedding from parallel plates: Calculation of resonant frequencies. J. Sound Vib. **5**, 330 (1967).
[33] N. A. Cumpsty and D. S. Whitehead, The excitation of acoustic resonances by vortex shedding. J. Sound Vib. **18**, 353 (1971).
[34] W. Koch, Resonant acoustic frequencies of flat plate cascades. J. Sound Vib. **88**, 233 (1983).
[35] R. Parker and S. A. T. Stoneman, The excitation and consequences of acoustic resonances in enclosed fluid flow around solid bodies, Proc. Inst. Mech. Eng. C **203**, 9 (1989).
[36] D. V. Evans, M. Levitin, and D. Vassiliev, Existence theorems for trapped modes, J. Fluid Mech **261**, 21 (1994).
[37] P. Paddon and J. F. Young, Two-dimensional vector-coupled-mode theory for textured planar waveguides, Phys. Rev. B **61**, 2090 (2000).
[38] V. Pacradouni, W. J. Mandeville, A. R. Cowan, P. Paddon, J. F. Young, and S. R. Johnson, Photonic band structure of dielectric membranes periodically textured in two dimensions, Phys. Rev. B **62**, 4204 (2000).
[39] T. Ochiai and K. Sakoda, Dispersion relation and optical transmittance of a hexagonal photonic crystal slab, Phys. Rev. B **63**, 125107 (2001).
[40] S. Fan and J. D. Joannopoulos, Analysis of guided resonances in photonic crystal slabs, Phys. Rev. B **65**, 235112 (2002).
[41] C. W. Hsu, B. Zhen, S.-L. Chua, S. G. Johnson, J. D. Joannopoulos, and M. Soljačić, Bloch surface eigenstates within the radiation continuum, Light Sci. Appl. **2**, e84 (2013).
[42] C. W. Hsu, B. Zhen, J. Lee, S.-L. Chua, S. G. Johnson, J. D. Joannopoulos, and M. Soljačić, Observation of trapped light within the radiation continuum, Nature (London) **499**, 188 (2013).
[43] Y. Yang, C. Peng, Y. Liang, Z. Li, and S. Noda, Analytical Perspective for Bound States in the Continuum in Photonic Crystal Slabs, Phys. Rev. Lett. **113**, 037401 (2014).
[44] B. Zhen, C. W. Hsu, L. Lu, A. D. Stone, and M. Soljačić, Topological Nature of Optical Bound States in the Continuum, Phys. Rev. Lett. **113**, 257401 (2014).
[45] H. Zhou, B. Zhen, C. W. Hsu, O. D. Miller, S. G. Johnson, J. D. Joannopoulos, and M. Soljačić, Perfect single-sided radiation and absorption without mirrors, Optica **3**, 1079 (2016).
[46] X. Gao, C. W. Hsu, B. Zhen, X. Lin, J. D. Joannopoulos, M. Soljačić, and H. Chen, Formation mechanism of guided resonances and bound states in the continuum in photonic crystal slabs, Sci. Rep. **6**, 31908 (2016).
[47] A. Kodigala, T. Lepetit, Q. Gu, B. Bahari, Y. Fainman, and B. Kanté, Lasing action from photonic bound states in continuum, Nature (London) **541**, 196 (2017).
[48] W. Zhang, A. Charous, M. Nagai, D. M. Mittleman, and R. Mendis, Extraordinary optical reflection resonances and bound states in the continuum from a periodic array of thin metal plates, Opt. Express **26**, 13195 (2018).
[49] M. Minkov, I. A. D. Williamson, M. Xiao, and S. Fan, Zero-Index Bound States in the Continuum, Phys. Rev. Lett. **121**, 263901 (2018).
[50] A. Cerjan, C. W. Hsu, and M. C. Rechtsman, Bound States in the Continuum through Environmental Design, Phys. Rev. Lett. **123**, 023902 (2019).
[51] Y. Plotnik, O. Peleg, F. Dreisow, M. Heinrich, S. Nolte, A. Szameit, and M. Segev, Experimental Observation of Optical Bound States in the Continuum, Phys. Rev. Lett. **107**, 183901 (2011).
[52] S. Weimann, Y. Xu, R. Keil, A. E. Miroshnichenko, A. Tünnermann, S. Nolte, A. A. Sukhorukov, A. Szameit, and Y. S. Kivshar, Compact Surface Fano States Embedded in the Continuum of Waveguide Arrays, Phys. Rev. Lett. **111**, 240403 (2013).
[53] G. Corrielli, G. Della Valle, A. Crespi, R. Osellame, and S. Longhi, Observation of Surface States with Algebraic Localization, Phys. Rev. Lett. **111**, 220403 (2013).
[54] J. Gomis-Bresco, D. Artigas, and L. Torner, Anisotropy-induced photonic bound states in the continuum, Nat. Photonics **11**, 232 (2017).
[55] S. Mukherjee, J. Gomis-Bresco, P. Pujol-Closa, D. Artigas, and L. Torner, Topological properties of bound states in the continuum in geometries with broken anisotropy symmetry, Phys. Rev. A **98**, 063826 (2018).
[56] B.-J. Yang, M. Saeed Bahramy, and N. Nagaosa, Topological protection of bound states against the hybridization, Nat. Commun. **4**, 1524 (2013).
[57] Z.-G. Chen, C. Xu, R. Al Jahdali, J. Mei, and Y. Wu, Corner states in a second-order acoustic topological insulator as bound states in the continuum, Phys. Rev. B **100**, 075120 (2019).
[58] M. Robnik, A simple separable Hamiltonian having bound states in the continuum, J. Phys. A: Math. Gen. **19**, 3845 (1986).
[59] J. U. Nöckel, Resonances in quantum-dot transport, Phys. Rev. B **46**, 15348 (1992).
[60] F. Liu and K. Wakabayashi, Novel Topological Phase with a Zero Berry Curvature, Phys. Rev. Lett. **118**, 076803 (2017).
[61] See Supplemental Material at http://link.aps.org/supplemental/10.1103/PhysRevB.101.161116 for a detailed description of the topological phases and invariants in this model, the implementation of the symmetry-breaking terms added to the pristine Hamiltonian for Fig. 4, and scaling arguments for the BICs, which includes Refs. [65–67].
[62] Although a proper definition of corner-induced filling anomaly requires the vanishing of polarization in insulators, here we do not enforce this requirement as we envision the topology per band instead of the topology below a given Fermi level.
[63] In contrast, if the BICs were the result of adding losses into the environment $\mathcal{R}$, we would observe their modal profiles to

have a relatively uniform distribution over the entire lossless regions $\mathcal{S}$.

[64] Although the plot shows that the edge states are spectrally separated from the bulk bands only for a fraction of the topological phase, they persist up to the bulk transition point $|t| = 1$.

[65] G. H. Wannier, Dynamics of band electrons in electric and magnetic fields, Rev. Mod. Phys. **34**, 645 (1962).

[66] N. Marzari and D. Vanderbilt, Maximally localized generalized Wannier functions for composite energy bands, Phys. Rev. B **56**, 12847 (1997).

[67] B. Bradlyn, L. Elcoro, J. Cano, M. G. Vergniory, Z. Wang, C. Felser, M. I. Aroyo, and B. A. Bernevig, Topological quantum chemistry, Nature (London) **547**, 298 (2017).